Science
AAAS

Supplementary Materials for

NLR immune receptor–nanobody fusions confer plant disease resistance

Jiorgos Kourelis *et al*.

Corresponding author: Sophien Kamoun, sophien.kamoun@tsl.ac.uk

Science **379**, 934 (2023)
DOI: 10.1126/science.abn4116

The PDF file includes:

Other Supplementary Material for this manuscript includes the following:

Materials and Methods

Plant growth conditions

Wild type *Nicotiana benthamiana* were grown in Levingtons F2 compost in a glasshouse set at 24 °C day / 22 °C night, humidity 45–65%, with supplementary lighting when the weather conditions required it. The *N. benthamiana* line stably expressing C-terminally 4xHA tagged Rx was previously described (*41*).

Plasmid constructions

The Golden Gate Modular Cloning (MoClo) kit (*54*) and the MoClo plant parts kit (*55*) were used for cloning, and all vectors are from this kit unless specified otherwise. Cloning design and sequence analysis were done using Geneious Prime (v2022.2.2; https://www.geneious.com). Plasmid construction is described in **Table S1**. To target GFP we chose the widely used anti-GFP nanobody Enhancer, also known as cAbGFP4 and which has been isolated multiple times (*33*, *56*, *57*), Minimizer nanobody (*33*), and selected LaG-2, LaG-16, and LaG-24 nanobodies from the total of 25 nanobodies targeting GFP isolated by Fridy *et al*., 2010 (*34*). The structure of LaG-16 and Enhancer in complex with GFP has been resolved and shows how they bind distinct interfaces (*33*, *51*), and based on NMR spectroscopy LaG-2 and LaG-24 bind to another distinct GFP interface (*34*). The anti-mCherry nanobodies, LaM-1, LaM-2, LaM-3, LaM-4, LaM-6, and LaM-8 were isolated by Fridy *et al*., 2010 (*34*). The structure of LaM-2 and LaM-4 in complex with mCherry has been resolved, showing these bind distinct interfaces (*52*), but the interaction interface of the remaining anti-mCherry nanobodies is currently unknown. Mutationally stabilized versions of LaG-24 (D3Q, S49F/Q66K/D75N/H83Q/D85N/D86S/V88K), LaM-2 (T26A/V77A/S97Y), LaM-3 (Q8E/E67K/D68G/S79N/A80T), and LaM-6

(S42A/N45K/L49F/M73R/N86S/V87L/N88K/A89P) were designed based on Dingus *et al*., 2022 (*32*).

Transient gene-expression and cell death assays

Transient gene expression in *N. benthamiana* were performed by agroinfiltration according to methods described by van der Hoorn *et al.* 2000 . Briefly, *A. tumefaciens* strain GV3101 pMP90 carrying binary vectors were inoculated from glycerol stock in LB supplemented with appropriate antibiotics and grown O/N at 28 °C until saturation. Cells were harvested by centrifugation at 2000 × *g*, RT for 5 min. Cells were washed once and resuspended in infiltration buffer (10 mM $MgCl_2$, 10 mM MES-KOH pH 5.6, 200 µM acetosyringone) to the appropriate OD_{600} (see **Table S1**) in the stated combinations and left to incubate in the dark for 2h at RT prior to infiltration into 5-week-old *N. benthamiana* leaves. Two leaves from three plants were inoculated per experiment (N = 6), and the experiment was repeated three times. In all assays where the original Pikm was co-infiltrated with its cognate effector AVR-PikD, we co-infiltrated the *Tomato bushy stunt virus* (TBSV) silencing inhibitor p19 (*59*) to enhance expression and ensure reliable HR. Hypersensitive cell death phenotypes were visually scored 4-5 days post-infiltration in a range from 0 (no visible necrosis) to 7 (fully confluent necrosis) according to Adachi *et al.* 2019 (*60*). We followed the same procedure for cell death assays in *N. benthamiana* transgenic lines. The data was visualized with ggplot2 (v3.3.4) (*61*) and the statistical analysis was performed using the R package besthr (v0.2.0) (*53*) (**Table S2** for raw data).

Transgenic *N. benthamiana*

A. tumefaciens-mediated transformation of *N. benthamiana* was performed as described (*62*). Briefly, young leaves (up to 10 cm in diameter) of 4-week-old *N. benthamiana* plants were surface sterilised by brief dipping into 70% ethanol and then immersing into 1% fresh

sodium hypochlorite with a few drops of Tween 20 to act as a surfactant for 25 minutes. Leaves were then rinsed in sterile water and cut into 1-2 cm^2 sections. *A. tumefaciens* strain GV3101 pMP90 carrying binary plasmid pJK-B2-0528 (pL2M-NPTII//pMAS::Pikm-2-6xHA//2x35S::Pikm-1-HF) or pJK-B2-0529 (pL2M-NPTII//pMAS::Pikm-2-6xHA//2x35S::Pikm-$1^{Enhancer}$-HF) (cloning described in **Table S1**) were inoculated from glycerol stock in LB supplemented with appropriate antibiotics and grown O/N at 28 °C until saturation. Cells were harvested by centrifugation at 2000 × *g*, RT for 5 min. Cells were washed once and resuspended in the same volume of inoculation buffer (per liter: 4.3 g MS basal salts (1×), 30 g sucrose). Leave squares were fully immersed into the agrobacterium inoculation suspension, briefly blotted dry, and transferred to co-cultivation medium media [per liter: 4.3 g MS basal salts (1×), 30 g sucrose, 1× Gamborg's B5 vitamins, 0.1 mg Naphthalene Acetic Acid (NAA), 0.59 g MES, pH = 5.7 using KOH, 4 g Agargel] supplemented with 1 mg/L Benzylaminopurine (BAP). Plates were left for 3 days in a growth chamber (24 °C, 18-h light) before transferring explants to plates containing shooting media (co-cultivation medium media supplemented with 1 mg/L Benzylaminopurine (BAP), 500 µg/ml Cefotaxime/Augmentin, and 100 µg/ml kanamycin). Explants were subcultured onto fresh shooting media every 7-10 days for 1-2 months until the appearance of the first shoots. Shoots >3 mm were excised and transferred to rooting media [per liter: 2.15 g MS basal salts (0.5×), 5 g sucrose, pH = 5.8 with KOH, 2.5 g Gelrite] supplemented with 500 µg/ml Cefotaxime/Augmentin and 100 µg/ml kanamycin. Explants were further cultured until roots appeared after which plantlets were transferred to soil and grown in the glasshouse. T0 *N. benthamiana* transformants were screened via hypersensitive cell death assays by agroinfiltration of *A. tumefaciens* strains carrying binary plasmids for the expression of GFP, AVR-PikD, or mCherry, as described above (**Table S2**). All plants triggering an immune response to their cognate 'effector' were taken forward to generate T1 progenies (**Table S3**).

Protein immunoblotting

Six *N. benthamiana* leaf discs (9 mm diameter) taken 2 days post agroinfiltration were homogenised in 200 µL extraction buffer [10% glycerol, 25 mM Tris-HCl, pH 7.5, 1 mM EDTA, 150 mM NaCl, 2% (w/v) PVPP, 10 mM DTT, 1x protease inhibitor cocktail (SIGMA), 0.2% IGEPAL® CA-630 (SIGMA)]. The supernatant obtained after centrifugation at 5,600 x g for 10 min at 4 °C was used for SDS-PAGE. 4x SDS-PAGE sample buffer [final concentration: 50 mM Tris-HCl (pH 6.8), 100 mM DTT, 2% SDS, 0.01% bromophenol blue, 10% glycerol] was added and the samples were denatured by incubating at 72 °C for 10 min. Proteins were separated on 10-20%, SDS-PAGE gels (Bio-Rad) and transferred onto polyvinylidene difluoride (PVDF) membrane using a Trans-Blot turbo transfer system (Bio-Rad). Membranes were blocked in in 3% dried milk dissolved in Tris-buffered Saline [50mM Tris-HCL (pH7.5), 150mM NaCl] supplemented with 1% Tween® 20 for 30 min before probing the membrane with either rat monoclonal anti-HA antibody (3F10, Roche; 1:4000 dilution), mouse monoclonal ANTI-FLAG® antibody conjugated to HRP (M2, Sigma; 1:4000 dilution), mouse monoclonal anti-V5 antibody (V5-10, Sigma-Aldrich; 1:4000), mouse monoclonal anti-GFP antibody conjugated to HRP (B-2, Santa Cruz Biotech; 1:4000 dilution), or mouse monoclonal anti-mCherry TrueMAB™ antibody conjugated to HRP (OTI10G6, Thermo Fisher Scientific; 1:2500 dilution). Chemiluminescent detection of signals after addition of either Pierce™ ECL Western (Thermo Fisher Scientific), or 1/5 to ½ SuperSignal™ West Femto Maximum Sensitivity Substrate (34095, Thermo Fisher Scientific) was done using the ImageQuant LAS 4000 luminescent imager (GE Healthcare Life Sciences) in the transient assays or the Amersham™ ImageQuant™ 800 biomolecular imager in the *N. benthamiana* transgenic lines assays. Equal loading was validated by staining the PVDF membranes with Ponceau S.

PVX infection assays - agroinfiltration

Four to five-weeks old *N. benthamiana* plants were inoculated with *Potato virus X* (PVX) strains (*40, 42, 43*) expressing either GFP or mCherry by agroinfiltration as described above. The PVX expression constructs are detailed in **Table S1**. Two leaves from three plants were inoculated per experiment (N = 6) as in **Fig. 2E**, **F**, and the experiment was repeated three times in transient expression assays (see **Table S3** for raw data). For PVX infection in stable transgenic lines, we first screened 15 independent plants per T1 line by agroinfiltration as described above (**Fig. S9, Table S5**), and retained plants triggering a specific immune response to their cognate effector for subsequent PVX infection assays on different leaves of the same plant (**Fig. 4**, **Fig. S10**, **Table S6**). Two leaves from five plants were inoculated per experiment. GFP or mCherry fluorescence was measured 4-5 days post-infiltration using the ImageQuant LAS 4000 luminescent imager (GE Healthcare Life Sciences) with the appropriate excitation and emission settings (EX: epi-RGB, EM:510DF10 filter for GFP and EX: epi-Green, EM: 605DF40 for mCherry), or the Amersham™ ImageQuant™ 800 biomolecular imager (Cy2 450nm for GFP and Cy3 535 nm for mCherry). The mean fluorescence intensity per cm^2 in each infiltration site was measured using Fiji (ImageJ v2.1.0), and a Dunnett's test was conducted using the R package DescTools (v0.99.41) (*63*) to compare mean fluorescence intensity per cm^2 between buffer only (negative control) and all tested constructs. For the stacking of Pikobodies (Figure 3), we conducted an ANOVA and Tukey HSD post-hoc test using the R package agricolae to compare mean fluorescence intensity per cm^2 across all treatments (v1.3-5). The data was visualized using ggplot2 (v3.3.4) (*61*).

We used GFP or mCherry accumulation as a proxy for PVX load, and coat protein (CP) accumulation as a direct read-out of PVX load (**Fig. 4**, **Fig. S10**). For these experiments, six leaf discs from the same infiltration site at the same time-point were taken and processed as

above. Samples containing PVX expressed GFP or mCherry were diluted threefold in SDS-PAGE sample buffer to prevent saturation of the signal during detection. GFP, mCherry, and CP were probed with either mouse monoclonal anti-GFP antibody conjugated to HRP (B-2, Santa Cruz Biotech; 1:4000 dilution), mouse monoclonal anti-mCherry TrueMAB™ antibody conjugated to HRP (OTI10G6, Thermo Fisher Scientific; 1:2500 dilution), or rabbit polyclonal anti-CP antibody (CAB10000-1000, Agdia EMEA; 1:2000 dilution), respectively. Chemiluminescent detection of signals was done as above.

PVX infection assays – wound inoculation via toothpick

PVX inoculation via toothpick has been previously described (*64*). Briefly, *A. tumefaciens* strains expressing PVX-GFP and PVX-mCherry were grown densely on LB plates containing appropriate antibiotics for two days at 28 °C. A sterilized toothpick was then used to scrape bacterial colonies and pierce holes in *N. benthamiana* leaves followed by a rotating motion to deliver PVX. Four to five holes were pierced on one side of the leaf with PVX-GFP and the other side with PVX-mCherry (**Fig. 4**, **Fig. S11**). This layout was repeated on a total of ten leaves (two leaves per plant, five plants per line). Eight leaf discs were sampled at 7 dpi with a cork borer (6 mm diameter) centered on the toothpick hole for protein extraction and immunoblotting as described above, except that 150 µL protein extraction buffer was used to homogenize ground leaf samples.

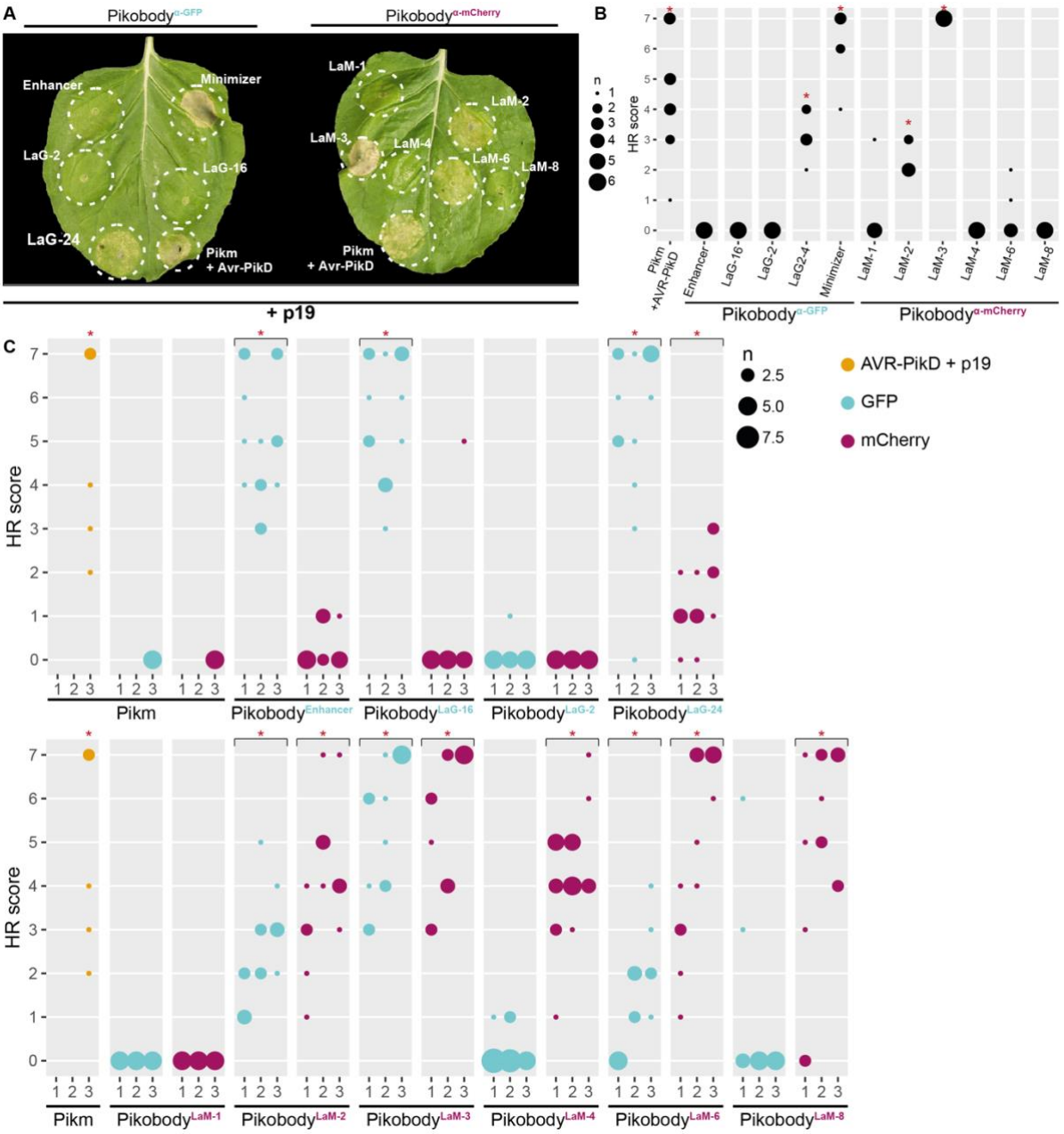

Fig. S1. Most tested Pikobodies are not autoimmune and trigger specific responses to their ligands. (**A**) Representative *N. benthamiana* leaf infiltrated with constructs indicated in white in the presence of the Tomato bushy stunt virus silencing inhibitor p19. Infiltration sites are circled with a white dashed line. Leaves were photographed 4 days after infiltration. (**B**) HR scores visualized as dots plot, where the size of a dot is proportional to the number of samples with the same score (n) within the same replicate (1 to 3). The experiment was repeated three times with six internal replicates; each column represents a combination of constructs (labelled on the bottom). Asterisks indicate statistically significant differences as compared to the corresponding control, as determined by the besthr R package **(*53*)**. (**C**) HR scores (representative images in **Fig. 1C**) visualized as dots plot, where the size of a dot is proportional to the number of samples with the same score (n) within the same

replicate (1 to 3). The experiment was repeated three times. Asterisks indicate statistically significant differences as compared to the corresponding control (Pikm + GFP), as determined by the besthr R package **(*53*)**.

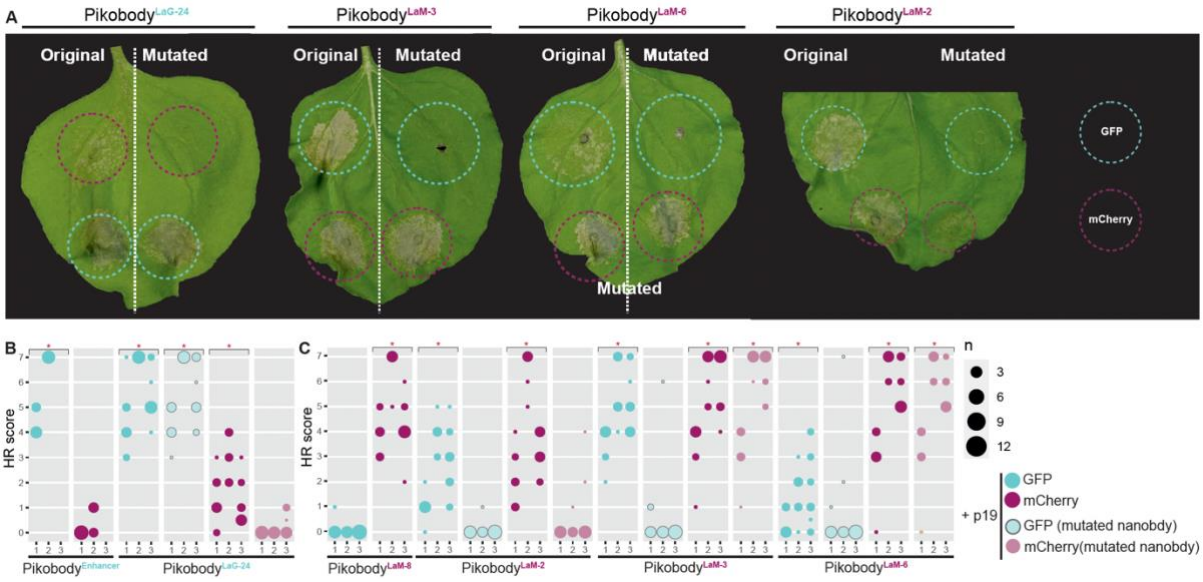

Fig. S2. Mutational stabilization of nanobodies abolishes Pikobody autoactivity. (**A**) Targeted mutation in shared structural motifs of the nanobody scaffold can abolish autoimmunity while preserving immune response to the matching fluorescent protein. Representative *N. benthamiana* leaves were infiltrated with indicated constructs in the presence of the Tomato bushy stunt virus silencing inhibitor p19 and photographed 5 days after infiltration. The original Pikobody^{LaG-24} fusion (α-GFP), or Pikobody^{LaM-3} and Pikobody^{LaM-6} fusions (α-mCherry) display autoimmunity characterized by HR in presence of non-matching FPs. Fusion of mutationally stabilized versions of these nanobodies into the Pikobody scaffold result in abolition of autoactivity while retaining activation in the presence of the correct FP. Mutational stabilization of LaM-2 results in loss of autoactivity, and loss of mCherry recognition. (**B-C**). HR scores are visualized as dots plot, where the size of a dot is proportional to the number of samples with the same score (n) within the same replicate (1 to 3). The experiment was repeated three times. Asterisks indicate statistically significant differences as compared to Pikobody^{Enhancer} co-infiltration with a mCherry control (**B**) or Pikobody^{LaM-8} co-infiltration with a GFP (**C**) as determined by the besthr R package (*53*).

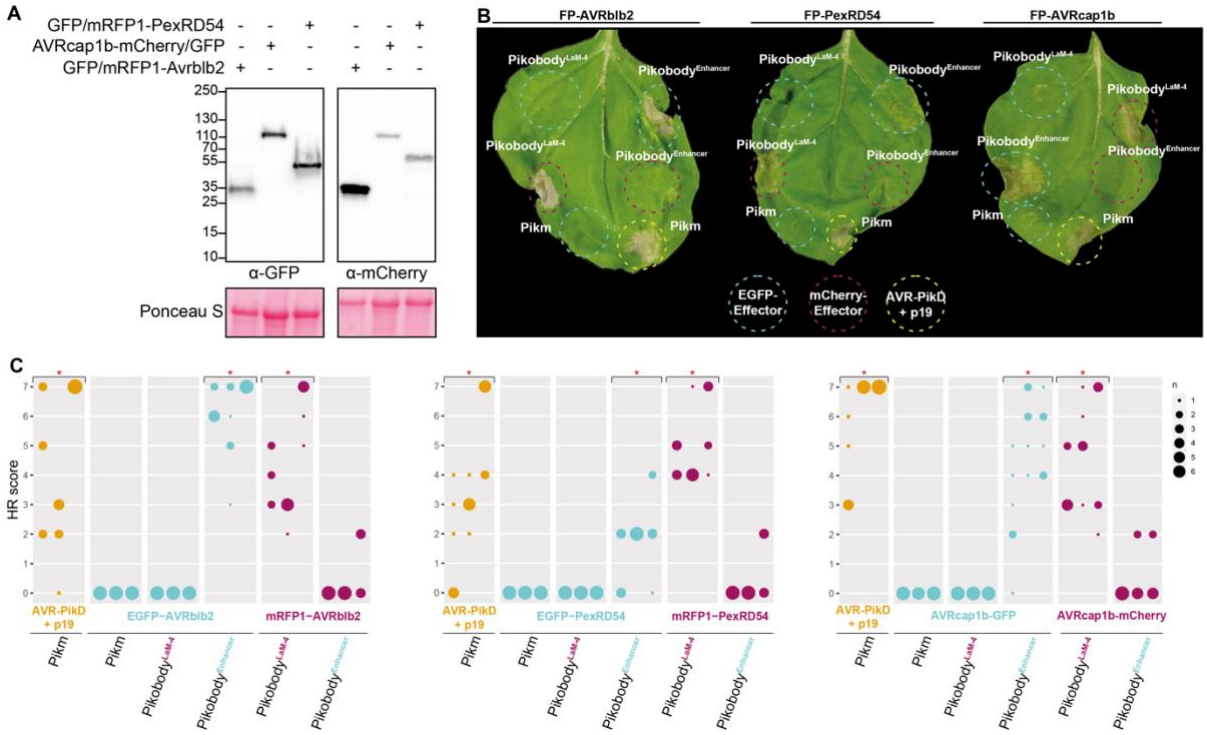

Fig. S3. Pikobodies specifically trigger HR in response to EGFP/GFP- or mRFP1/mCherry-tagged *Phytophthora infestans* effectors AVRblb2, PexRD54, or AVRcap1b. (**A**) Immunoblot detection of EGFP/GFP- or mRFP1/mCherry-tagged AVRblb2, AVRcap1b, and PexRD54 using using anti-GFP or anti-mCherry antibody, respectively. Ponceau S staining shows comparable protein loading across samples. Total protein was extracted 2 days after agroinfiltration of the stated constructs. (**B**) Pikobody^{Enhancer} and Pikobody^{LaM4} specifically recognize EGFP- or mRFP1-tagged AVRblb2, PexRD54, or AVRcap1b, respectively. Representative *N. benthamiana* leaf infiltrated with constructs indicated in white and infiltration sites circled with a dashed line. Leaves were photographed 4 days after infiltration. Cyan, magenta or yellow dashed lines show sites co-infiltrated with EGFP/GFP or mRFP1/mCherry tagged effectors, or AVR-PikD co-infiltrated with the Tomato bushy stunt virus silencing inhibitor p19, respectively. (**C**) HR scores visualized as dots plot, where the size of a dot is proportional to the number of samples with the same score (n) within the same replicate (1 to 3). The experiment was repeated three times with six internal replicates; each column represents a combination of constructs (labelled on the bottom). Asterisks indicate statistically significant differences as compared to Pikobody co-infiltration with a mismatched FP as a control as determined by the besthr R package (*53*).

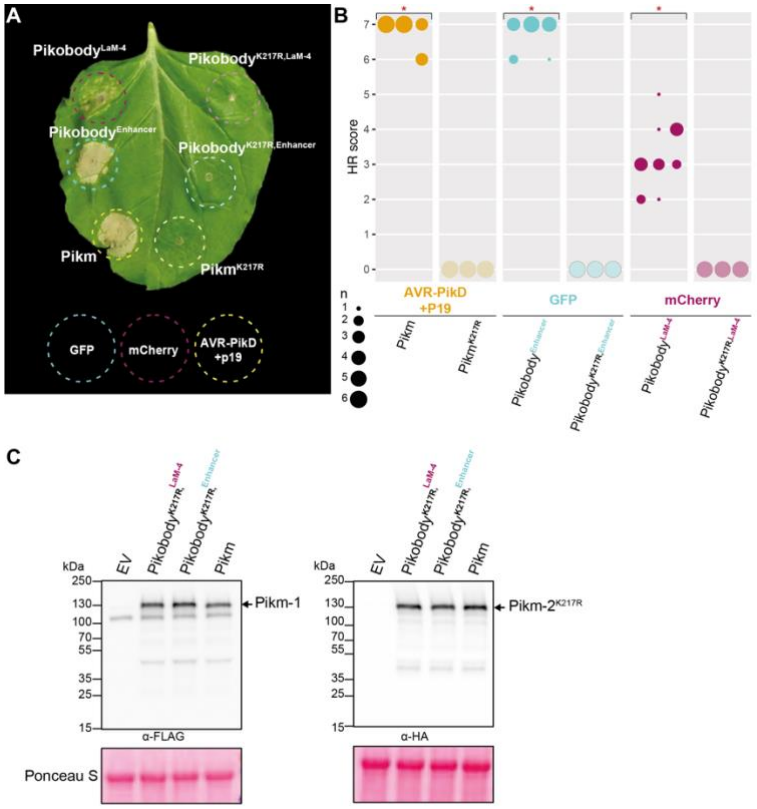

Fig. S4. Pikobody-mediated HR requires the Pikm-2 P-loop motif. (**A**) An intact Pikm-2 P-loop motif is required for Pikobody-mediated HR. Representative *N. benthamiana* leaf infiltrated with constructs indicated in white and infiltration sites circled with a dashed line. Leaves were photographed 4 days after infiltration. Cyan, magenta or yellow dashed lines shows sites co-infiltrated with GFP, mCherry or AVR-PikD co-infiltrated with the Tomato bushy stunt virus silencing inhibitor p19, respectively. Wild-type Pikm pair co-expressed with cognate effector AVR-PikD and silencer suppressor p19 was used as a positive control and Pikm^{K217R} P-loop mutant (mutation in Pikm-2) co-expressed with cognate effector AVR-PikD and silencer suppressor p19 was used as a negative control. (**B**) HR scores visualized as dots plot, where the size of a dot is proportional to the number of samples with the same score (n) within the same replicate (1 to 3). The experiment was repeated three times with six internal replicates; each column represents a combination of constructs (labelled on the bottom). Asterisks indicate statistically significant differences using Pikm^{K217R} P-loop mutant as a control as determined by the besthr R package (*53*). (**C**) Pikm-2^{K217R} P-loop mutant protein accumulates. For the immunoblot analysis, total protein was extracted 2 days after transient expression of Pikobody^{Enhancer}, Pikobody^{LaM4} and the wild-type Pikm pair. Pikm-1 and the Pikm-1 Enhancer and LaM-4 were C-terminally 6xHis-3xFLAG-tagged and detected using anti-FLAG antibody, while Pikm-2^{K217R} was C-terminally 6xHA-tagged and detected using anti-HA antibody. Empty vector was used as a negative control. Black arrows point to the band corresponding to Pikm-1 (anti-FLAG blot) and Pikm-2^{K217R} (anti-HA blot).

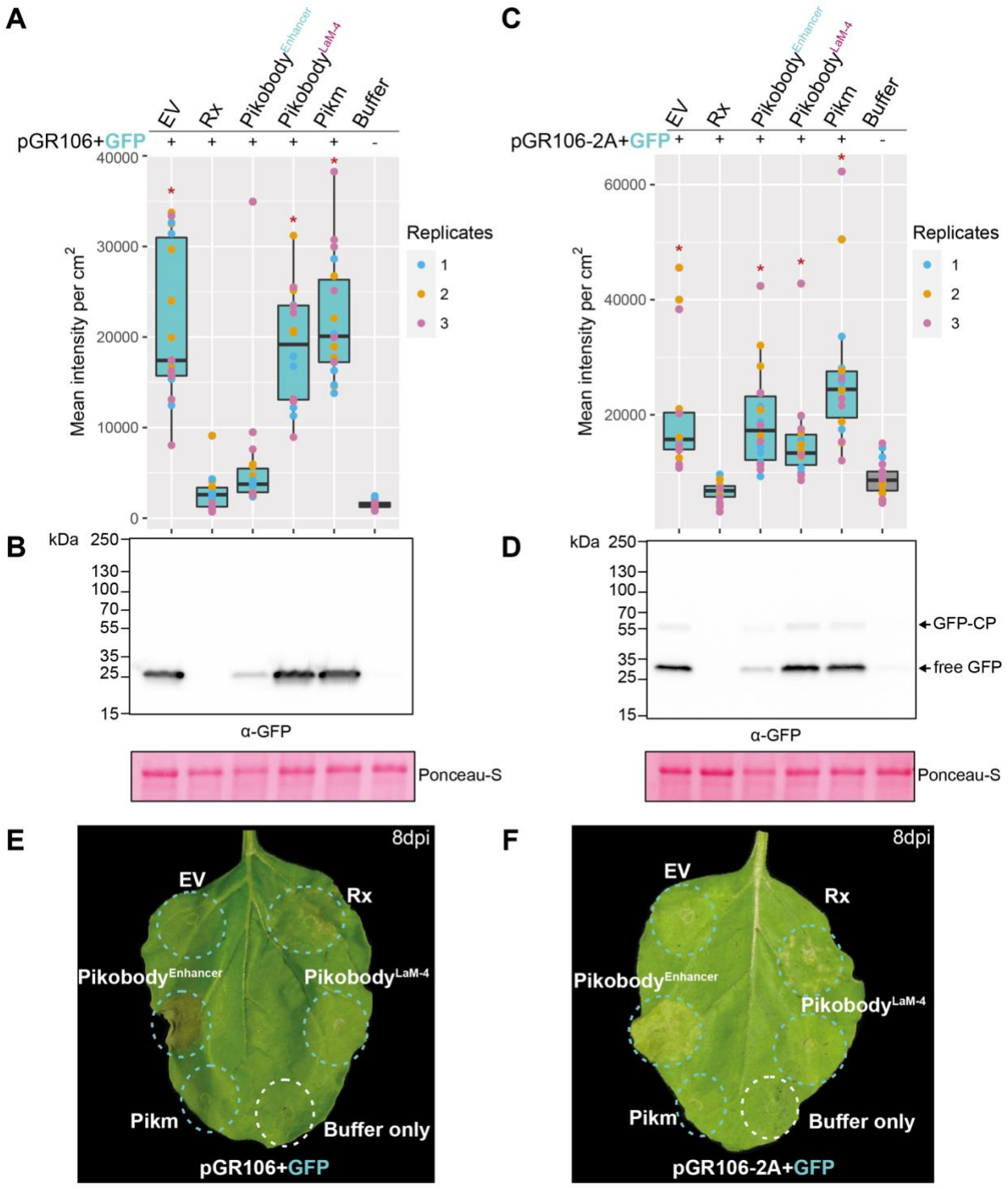

Fig. S5. Pikobody^{Enhancer} confers resistance against variants of Potato Virus X expressing GFP. (**A**) Specific reduction in fluorescence intensity of PVX expressed GFP in the presence of Pikobody^{Enhancer}. GFP mean fluorescence

intensity per cm^2 measured in *N. benthamiana* leaves 4 days post-infiltration was used as a proxy for PVX viral load in each infiltration site for a PVX variant expressing GFP from between the triple gene block and the coat protein (pGR106-GFP). The boxplot summarizes data obtained in three independent experiments (replicates) with six infiltration site per construct and per experiment. Red asterisks show significant differences between Buffer only (no PVX added, negative control) and tested constructs in the presence of pGR106-GFP (Dunnett's test, pvalue < 0.001). Empty vector was used as a positive control for viral load and Buffer only as a negative control for viral load. We also used Rx, a resistance gene recognizing the coat protein from PVX as a positive control for PVX resistance. (**B**) Specific reduction of PVX expressed GFP accumulation in the presence of Pikobody^{Enhancer}. GFP accumulation was used as proxy to evaluate viral load from pGR106-GFP. For the immunoblot analysis, total protein was extracted 2 days after inoculation with pGR106-GFP in the presence of the tested constructs. Empty vector was used as a positive control for viral load and Buffer only as a negative control. GFP was detected using anti-GFP antibody. Ponceau S staining shows equal protein loading across samples. (**C**) No reduction in fluorescence intensity of PVX expressed GFP fused to the coat protein in the presence of Pikobody^{Enhancer}. GFP mean fluorescence intensity per cm^2 measured in *N. benthamiana* leaves 4 days post-infiltration was used as a proxy for PVX viral load in each infiltration site for a PVX variant expressing GFP fused to the coat protein using the porcine teschovirus-1 2A "self-cleaving" peptide (pGR106-2A-GFP) leading to approximately 50 % of free GFP and 50 % of GFP fused to the viral coat protein (CP). Boxplots and analysis as in (**A**). (**D**) Specific reduction of PVX expressed GFP accumulation fused to the coat protein in the presence of Pikobody^{Enhancer}. GFP accumulation was used as proxy to evaluate viral load from pGR106-2A-GFP. Immunoblot analysis as in (**B**) with black arrows pointing to GFP fused to coat protein (GFP-CP) and free GFP. (**E-F**) Specific HR triggered by the two version of PVX expressing GFP in the presence of Pikobody^{Enhancer}. Representative *N. benthamiana* leaves infiltrated with appropriate constructs and photographed 8 days after infiltration. The delay in observing HR symptoms was due to the efficient elimination of PVX without visible HR at first, and the continuous production of PVX via agroinfiltration ultimately lead to HR in the late stages of infection. The infiltration site for each construct is labelled on the picture and circled with a yellow or white dashed line for pGR106+GFP (**E**) and pGR106-2A+GFP (**F**) or no PVX, respectively.

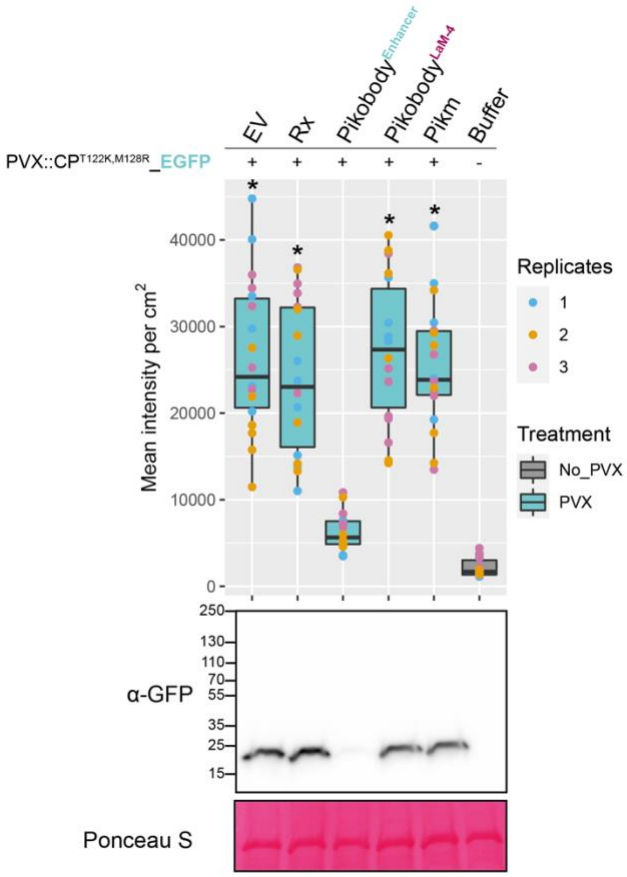

Fig. S6. Pikobody^{Enhancer} confers resistance against a PVX variant not recognized by Rx. (**A**) Boxplots show specific reduction in fluorescence intensity of PVX expressed GFP in the presence of Pikobody^{Enhancer} for PVX::CP^{T122K,M128R}. GFP mean fluorescence intensity per cm^2 measured in *N. benthamiana* leaves 4 days post-infiltration was used as a proxy for PVX viral load in each infiltration site for PVX expressing GFP. The boxplot summarizes data obtained in three independent experiments (replicates) with six infiltration site per construct and per experiment. Black asterisks show significant differences between Buffer only (no PVX added, negative control) and tested constructs in the presence of PVX-GFP (Dunnett's test, pvalue < 0.001). Empty vector was used as a positive control for viral load and Buffer only as a negative control for viral load. (**B**) Specific reduction of PVX expressed GFP accumulation in the presence of Pikobody^{Enhancer}. GFP accumulation was used as proxy to evaluate viral load from PVX-GFP. For the immunoblot analysis, total protein was extracted 4 days after inoculation with PVX-GFP in the presence of the tested constructs. Empty vector was used as a positive control for viral load and Buffer only as a negative control. GFP was detected using anti-GFP antibody. Ponceau S staining shows equal protein loading across samples

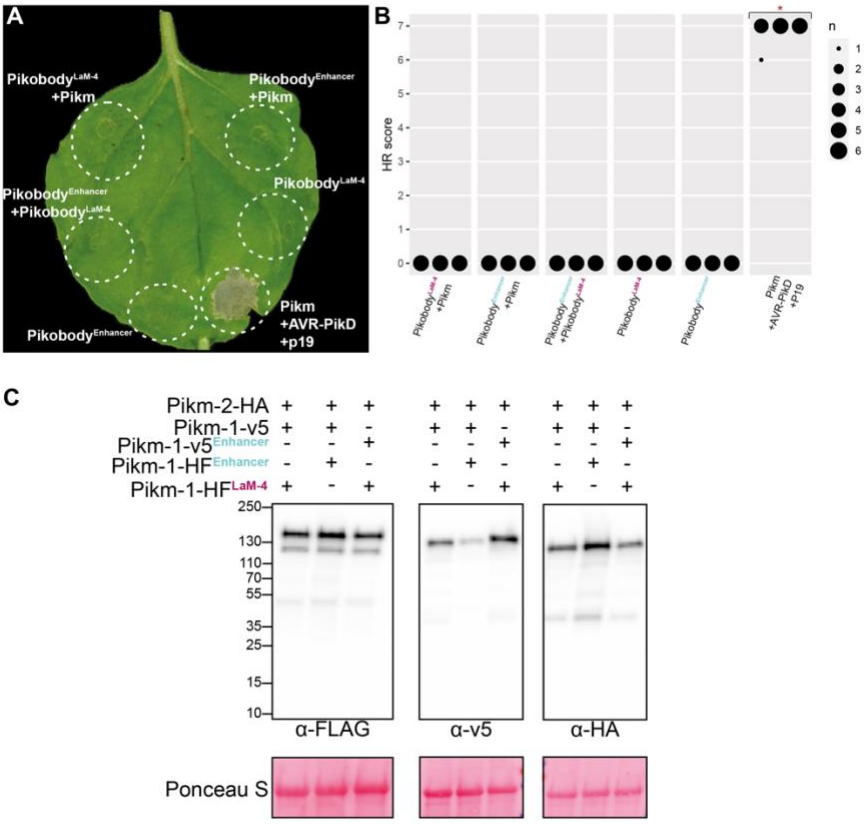

Fig. S7. Co-expressed Pikobodies are not autoactive. (**A**) Stacking of Pikobodies does not result in autoimmunity. Representative *N. benthamiana* leaf infiltrated with constructs indicated in white and infiltration sites circled with a white dashed line. Leaves were photographed 4 days after infiltration. (**B**) HR scores visualized as dots plot, where the size of a dot is proportional to the number of samples with the same score (n) within the same replicate (1 to 3). The experiment was repeated three times with six internal replicates; each column represents a combination of constructs (labelled on the bottom). Wild-type Pikm pair co-expressed with cognate effector AVR-PikD and silencer suppressor p19 was used as a positive control and Pikobody^{Enhancer} or Pikobody^{LaM4} expressed on their own as negative controls. Asterisks indicate statistically significant differences to all other treatments as determined by the besthr R package (*53*). (**C**) Pikobody stacking does not affect protein accumulation. For the immunoblot analysis, total protein was extracted 2 days after transient expression of Pikobody^{Enhancer}, Pikobody^{LaM4} and the wild-type Pikm pair. Pikm-1 and the Pikm-1 Enhancer and LaM-4 were either C-terminally 6xHis-3xFLAG- or V5-tagged and detected using anti-FLAG or anti-V5 antibody, respectively. Pikm-2 was C-terminally 6xHA-tagged and detected using anti-HA antibody.

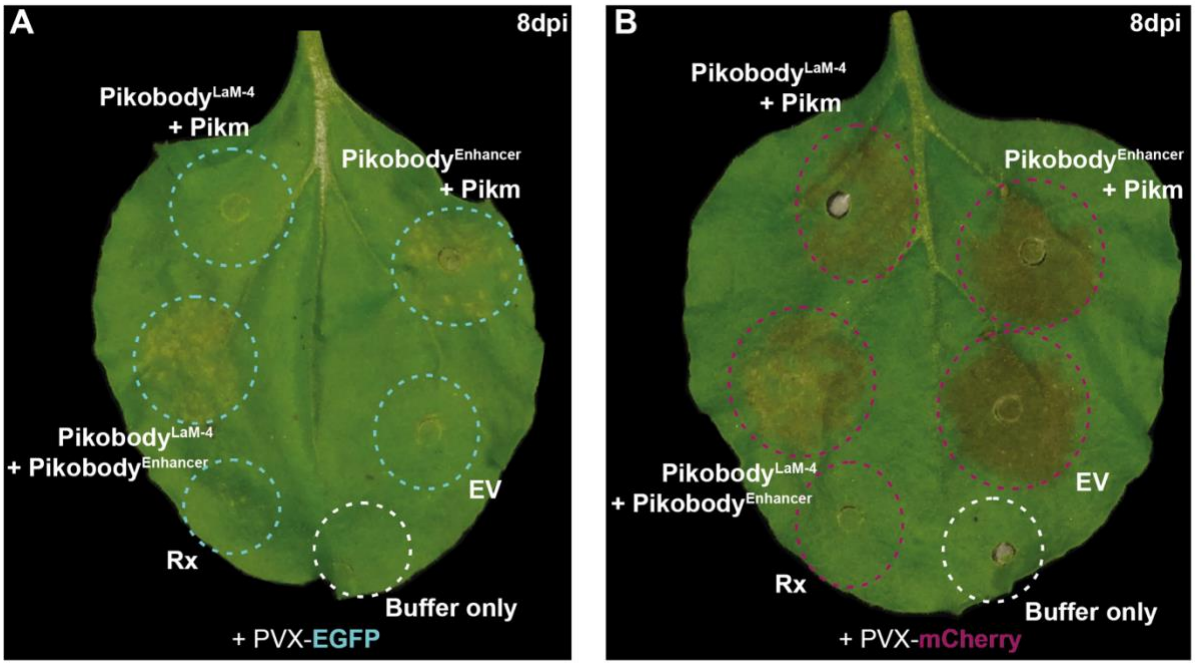

Fig. S8. PVX-triggered hypersensitive response (HR) phenotypes observed with stacked Pikobodies. (**A-B**) Specific HR triggered by PVX expressed EGFP (GFP, **A**) or mCherry (**B**) in the presence of stacked Pikobody^{Enhancer} and Pikobody^{LaM4}, respectively. Representative *N. benthamiana* leaves infiltrated with appropriate constructs and photographed 7 days after infiltration. The infiltration site for each construct is labelled on the picture and all sites but "Buffer only" were co-infiltrated with PVX-GFP (left) or PVX-mCherry (right). Cyan, magenta and white dashed lines depict the sites infiltrated with PVX-GFP, PVX-mCherry or no PVX, respectively. The purple color on the infiltration sites on (**B**) is due to a high expression of mCherry.

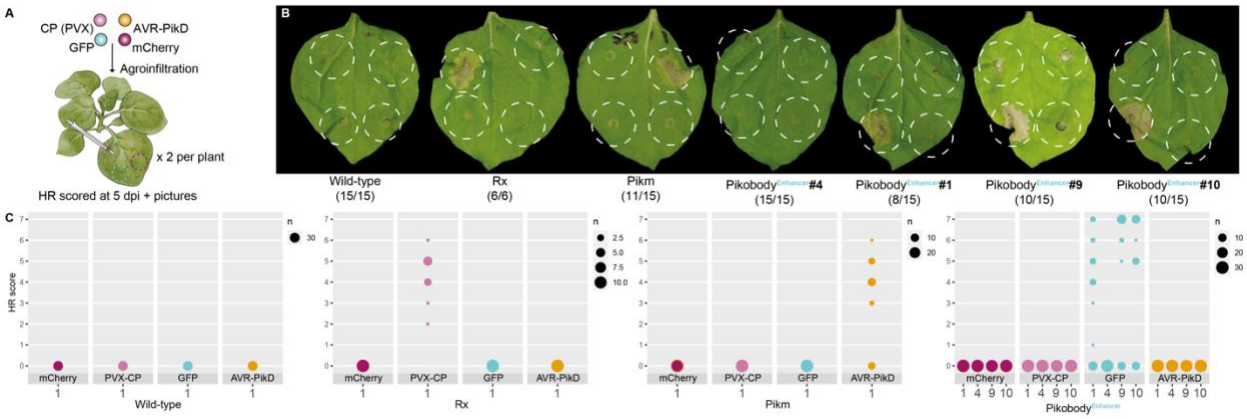

Fig. S9. Transgenic *N. benthamiana* lines stably expressing Pikobody^{Enhancer} trigger an immune response specifically in presence of GFP. (**A**) Schematics of the infiltration layout. (**B**) Representative *N. benthamiana* leaf for each line tested infiltrated with constructs indicated in (**A**). Leaves were photographed 4 days after infiltration and the numbers at the bottom represent the number of plants displaying the phenotype showed on the picture. (**C**) HR scores visualized as dots plot, where the size of a dot is proportional to the number of samples with the same score (n). We screened 15 plants for each newly generated T1 line (Pikm and Pikobody^{Enhancer} lines #1,#4,#9 and #10), given that we expect the transgene to be segregating. We also included as controls wild-type *N. benthamiana* and six plants for the Rx transgenic line (*41*). Each column represents an infiltrated construct (labelled on the bottom). Wild-type *N. benthamiana* and Pikobody^{Enhancer} #4 were used as a negative control for immune response and the Rx line was used as a positive control for immune response in presence of PVX coat protein specifically.

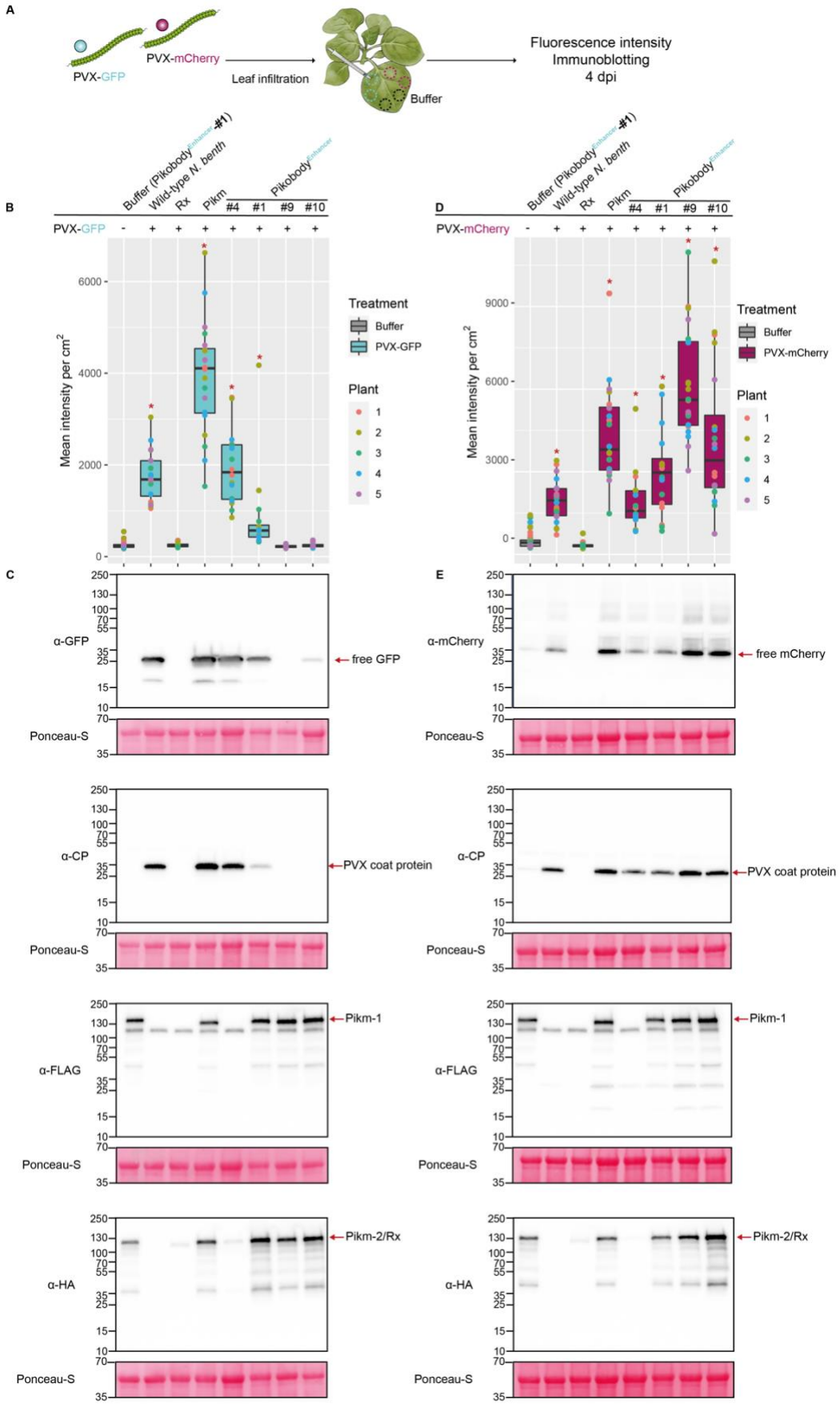

Fig. S10. Pikobody^{Enhancer} lines #9 and #10 confer specific resistance to PVX-GFP delivered by agroinfiltration.

(**A**) Experimental design of PVX resistance assay in transgenic *N. benthamiana* lines. (**B, D**) Specific reduction in fluorescence intensity of PVX expressed GFP (**B**), but not PVX-mCherry (**D**), in Pikobody^{Enhancer} line #9 and #10. GFP mean fluorescence intensity per cm^2 measured in *N. benthamiana* leaves 4 days post-infiltration was used as a proxy for PVX viral load in each infiltration site for PVX expressing GFP. The boxplot summarizes data obtained from five plants with two infiltration sites per construct. Red asterisks show significant differences between Buffer only (no PVX added, negative control) and tested constructs in the presence of PVX-GFP or PVX-mCherry (Dunnett's test, pvalue < 0.001). Wild-type *N. benthamiana* and a Pikm transgenic line were used as a negative control for PVX resistance (accumulation of both PVX variants) and Buffer only as a negative control for viral load. We also used transgenic *N. benthamiana* expressing Rx, a resistance gene recognizing the coat protein from PVX as a positive control for PVX resistance (no accumulation of either PVX variants). (**C**) Full blots of results displayed in **Fig. 4**. Specific reduction of PVX expressed GFP and coat protein accumulation in the presence of Pikobody^{Enhancer} line #9 and #10. GFP accumulation was used as proxy to evaluate viral load from PVX-GFP, which was further confirmed using an antibody targeting PVX coat protein. For the immunoblot analysis, total protein was extracted from the tested lines 4 days after inoculation with PVX-GFP or PVX-mCherry. Wild-type *N. benthamiana* and Pikm transgenic line were used as a positive control for viral load and Buffer only as a negative control (infiltrated in Pikobody^{Enhancer} #1 line). Antibody targeting FLAG was used to detect Pikm-1^{Enhancer} and Pikm-1, and antibody targeting HA was used to detect the presence of Pikm-2 and Rx. Ponceau S staining shows equal protein loading across samples. (**E**) Pikobody^{Enhancer} line #9 and #10 are not resistant to PVX-mCherry, unlike Rx transgenic lines. mCherry accumulation was used as proxy to evaluate viral load from PVX-mCherry, which was further confirmed using an antibody targeting PVX coat protein. Immunoblot analysis was done as in (**C**)

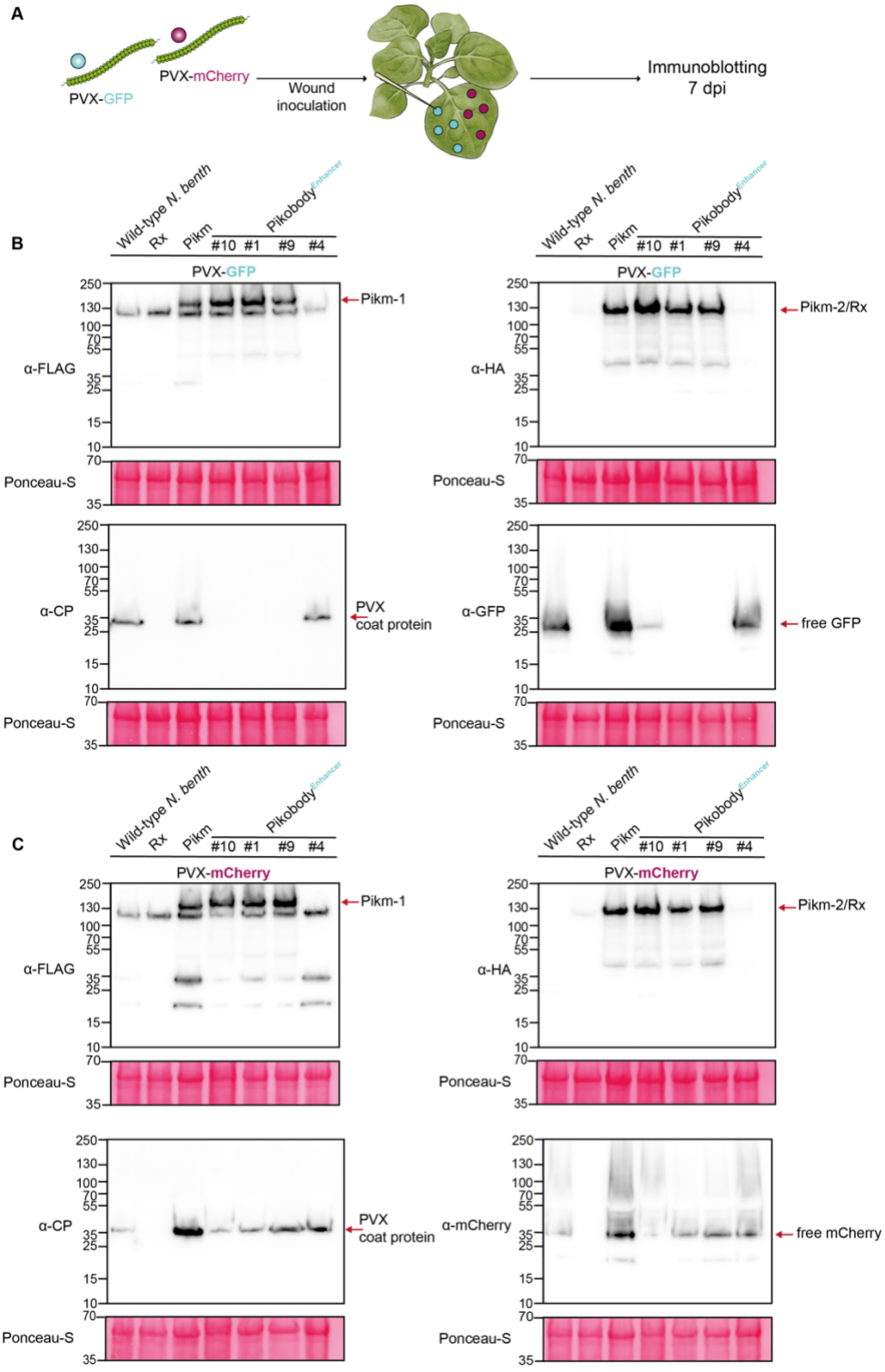

Fig. S11. Pikobody^{Enhancer} lines #1, #9, and #10 confer specific resistance to PVX-GFP delivered by wound inoculation. (**A**) Experimental design of PVX resistance assay in transgenic *N. benthamiana* lines. (**B**) Specific reduction of PVX expressed GFP and coat protein accumulation in the presence of Pikobody^{Enhancer} line #1, #9, and #10. GFP accumulation was used as proxy to evaluate viral load from PVX-GFP, which was further confirmed using

an antibody targeting PVX coat protein. For the immunoblot analysis, total protein was extracted from the tested lines 7 days after wound inoculation via toothpick with PVX-GFP. Wild-type *N. benthamiana* and Pikm transgenic line were used as a positive control for viral load and Buffer only as a negative control (infiltrated in Pikobody^{Enhancer1} line). Antibody targeting FLAG was used to detect Pikm-1^{Enhancer} and Pikm-1, and antibody targeting HA was used to detect the presence of Pikm-2 and Rx. Ponceau S staining shows equal protein loading across samples. (**C**) Pikobody^{Enhancer} line #1, #9, and #10 are not resistant to PVX-mCherry delivered by wound inoculation via toothpick, unlike Rx transgenic lines. mCherry accumulation was used as proxy to evaluate viral load from PVX-mCherry, which was further confirmed using an antibody targeting PVX coat protein. Immunoblot analysis was done as in (**C**)

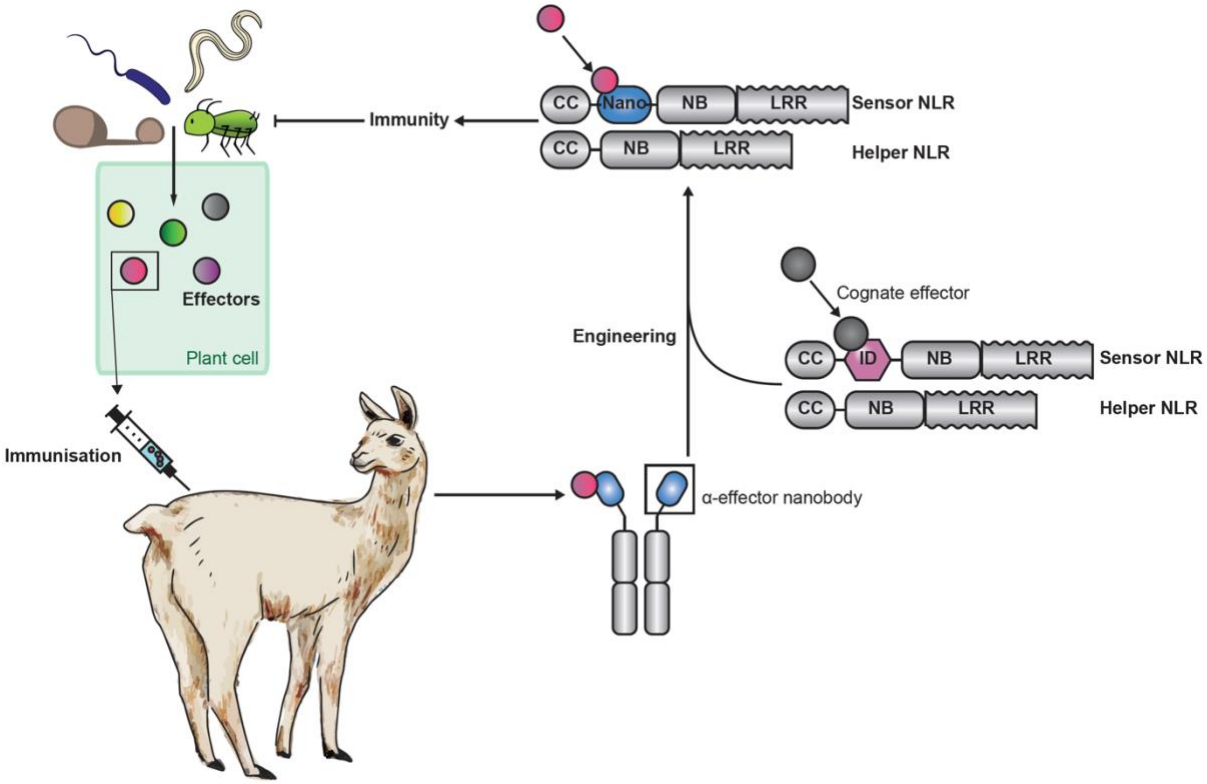

Figure S12: Pipeline for the generation of made-to-order functional Pikobodies. Immunization of camelids with translocated pathogen effectors generates nanobodies which can be integrated into the Pikm scaffold to generate functional Pikobodies providing immunity against pathogens translocating these effectors.

Table S1: Description of constructs and *A. tumefaciens* strains. Details of the constructs used in this study with associated selection antibiotic, purpose, publication, *A. tumefaciens* strain and OD_{600} used for infiltrations.

Table S2: Hypersensitive cell death quantification. HR scores reported by construct, experiment replicate (Experiment# in the table) and associated figure. We described HR scoring in the corresponding section of the Materials and Methods.

Table S3: Hypersensitive cell death quantification in *N. benthamiana* transgenic lines at the T0 stage. HR scores reported by transgenic line, individual plant and construct delivered via agroinfiltration. We described HR scoring in the corresponding section of the Materials and Methods. Lines selected to generate T1 are listed in the "Comment" column.

Table S4: Fluorescence intensity quantification for all transient assays with PVX-GFP and PVX-mCherry. Fluorescence intensity recorded for each infiltration site with the ImageQuant LAS 4000 luminescent imager (GE Healthcare Life Sciences) as described in the corresponding Materials and Methods section. Each line represents a construct co-infiltrated with a given PVX strain or no PVX (buffer only) with corresponding fluorescence per cm^2 measured in each infiltration site. We indicated the different experiment replicates in the column "Experiment#" and the corresponding figures in the last two columns.

Table S5: Hypersensitive cell death quantification in *N. benthamiana* transgenic lines. HR scores reported by transgenic line, individual plant and construct delivered via agroinfiltration. We described HR scoring in the corresponding section of the Materials and Methods.

Table S6: Fluorescence intensity quantification in *N. benthamiana* transgenic lines at the T1 stage. Fluorescence intensity recorded for each infiltration site with the Amersham™ ImageQuant™ 800 biomolecular imager as described in the corresponding Materials and Methods section. Each line represents a line infiltrated with a given PVX strain or no PVX (buffer only) with corresponding fluorescence per cm^2 measured in each infiltration site. We indicated the corresponding Figures in the last column.

References and Notes

1. S. H. Kim, D. Qi, T. Ashfield, M. Helm, R. W. Innes, Using decoys to expand the recognition specificity of a plant disease resistance protein. *Science* **351**, 684–687 (2016). doi:10.1126/science.aad3436 Medline

2. S. E. Pottinger, A. Bak, A. Margets, M. Helm, L. Tang, C. Casteel, R. W. Innes, Optimizing the PBS1 decoy system to confer resistance to potyvirus infection in *Arabidopsis* and soybean. *Mol. Plant Microbe Interact.* **33**, 932–944 (2020). doi:10.1094/MPMI-07-19-0190-R Medline

3. M. E. Segretin, M. Pais, M. Franceschetti, A. Chaparro-Garcia, J. I. B. Bos, M. J. Banfield, S. Kamoun, Single amino acid mutations in the potato immune receptor R3a expand response to *Phytophthora* effectors. *Mol. Plant Microbe Interact.* **27**, 624–637 (2014). doi:10.1094/MPMI-02-14-0040-R Medline

4. A. Giannakopoulou, J. F. C. Steele, M. E. Segretin, T. O. Bozkurt, J. Zhou, S. Robatzek, M. J. Banfield, M. Pais, S. Kamoun, Tomato I2 immune receptor can be engineered to confer partial resistance to the oomycete *Phytophthora infestans* in addition to the fungus *Fusarium oxysporum*. *Mol. Plant Microbe Interact.* **28**, 1316–1329 (2015). doi:10.1094/MPMI-07-15-0147-R Medline

5. J. C. De la Concepcion, M. Franceschetti, D. MacLean, R. Terauchi, S. Kamoun, M. J. Banfield, Protein engineering expands the effector recognition profile of a rice NLR immune receptor. *eLife* **8**, e47713 (2019). doi:10.7554/eLife.47713 Medline

6. S. Césari, Y. Xi, N. Declerck, V. Chalvon, L. Mammri, M. Pugnière, C. Henriquet, K. de Guillen, V. Chochois, A. Padilla, T. Kroj, New recognition specificity in a plant immune receptor by molecular engineering of its integrated domain. *Nat. Commun.* **13**, 1524 (2022). doi:10.1038/s41467-022-29196-6 Medline

7. S. Wang, W. Huang, Z. Duxbury, S. A. Hogenhout, J. D. G. Jones, Novel effector recognition capacity engineered into a paired NLR complex. bioRxiv 2021.09.06.459143 [Preprint] (2021). https://doi.org/10.1101/2021.09.06.459143.

8. J. L. Dangl, D. M. Horvath, B. J. Staskawicz, Pivoting the plant immune system from dissection to deployment. *Science* **341**, 746–751 (2013). doi:10.1126/science.1236011 Medline

9. S. Césari, M. Bernoux, P. Moncuquet, T. Kroj, P. N. Dodds, A novel conserved mechanism for plant NLR protein pairs: The “integrated decoy” hypothesis. *Front. Plant Sci.* **5**, 606 (2014). doi:10.3389/fpls.2014.00606 Medline

10. C.-H. Wu, K. V. Krasileva, M. J. Banfield, R. Terauchi, S. Kamoun, The “sensor domains” of plant NLR proteins: More than decoys? *Front. Plant Sci.* **6**, 134 (2015). doi:10.3389/fpls.2015.00134 Medline

11. T. Kroj, E. Chanclud, C. Michel-Romiti, X. Grand, J.-B. Morel, Integration of decoy domains derived from protein targets of pathogen effectors into plant immune receptors is widespread. *New Phytol.* **210**, 618–626 (2016). doi:10.1111/nph.13869 Medline

12. P. F. Sarris, V. Cevik, G. Dagdas, J. D. G. Jones, K. V. Krasileva, Comparative analysis of plant immune receptor architectures uncovers host proteins likely targeted by pathogens. *BMC Biol.* **14**, 8 (2016). doi:10.1186/s12915-016-0228-7 Medline

13. S. Césari, G. Thilliez, C. Ribot, V. Chalvon, C. Michel, A. Jauneau, S. Rivas, L. Alaux, H. Kanzaki, Y. Okuyama, J.-B. Morel, E. Fournier, D. Tharreau, R. Terauchi, T. Kroj, The rice resistance protein pair RGA4/RGA5 recognizes the *Magnaporthe oryzae* effectors AVR-Pia and AVR1-CO39 by direct binding. *Plant Cell* **25**, 1463–1481 (2013). doi:10.1105/tpc.112.107201 Medline

14. P. F. Sarris, Z. Duxbury, S. U. Huh, Y. Ma, C. Segonzac, J. Sklenar, P. Derbyshire, V. Cevik, G. Rallapalli, S. B. Saucet, L. Wirthmueller, F. L. H. Menke, K. H. Sohn, J. D. G. Jones, A plant immune receptor detects pathogen effectors that target WRKY transcription factors. *Cell* **161**, 1089–1100 (2015). doi:10.1016/j.cell.2015.04.024 Medline

15. C. Le Roux, G. Huet, A. Jauneau, L. Camborde, D. Trémousaygue, A. Kraut, B. Zhou, M. Levaillant, H. Adachi, H. Yoshioka, S. Raffaele, R. Berthomé, Y. Couté, J. E. Parker, L. Deslandes, A receptor pair with an integrated decoy converts pathogen disabling of transcription factors to immunity. *Cell* **161**, 1074–1088 (2015). doi:10.1016/j.cell.2015.04.025 Medline

16. A. Maqbool, H. Saitoh, M. Franceschetti, C. E. M. Stevenson, A. Uemura, H. Kanzaki, S. Kamoun, R. Terauchi, M. J. Banfield, Structural basis of pathogen recognition by an integrated HMA domain in a plant NLR immune receptor. *eLife* **4**, e08709 (2015). doi:10.7554/eLife.08709 Medline

17. L. Guo, S. Césari, K. de Guillen, V. Chalvon, L. Mammri, M. Ma, I. Meusnier, F. Bonnot, A. Padilla, Y.-L. Peng, J. Liu, T. Kroj, Specific recognition of two MAX effectors by integrated HMA domains in plant immune receptors involves distinct binding surfaces. *Proc. Natl. Acad. Sci. U.S.A.* **115**, 11637–11642 (2018). doi:10.1073/pnas.1810705115 Medline

18. T. K. Eitas, J. L. Dangl, NB-LRR proteins: Pairs, pieces, perception, partners, and pathways. *Curr. Opin. Plant Biol.* **13**, 472–477 (2010). doi:10.1016/j.pbi.2010.04.007 Medline

19. I. Ashikawa, N. Hayashi, H. Yamane, H. Kanamori, J. Wu, T. Matsumoto, K. Ono, M. Yano, Two adjacent nucleotide-binding site–leucine-rich repeat class genes are required to confer *Pikm*-specific rice blast resistance. *Genetics* **180**, 2267–2276 (2008). doi:10.1534/genetics.108.095034 Medline

20. H. Kanzaki, K. Yoshida, H. Saitoh, K. Fujisaki, A. Hirabuchi, L. Alaux, E. Fournier, D. Tharreau, R. Terauchi, Arms race co-evolution of *Magnaporthe oryzae AVR-Pik* and rice *Pik* genes driven by their physical interactions. *Plant J.* **72**, 894–907 (2012). doi:10.1111/j.1365-313X.2012.05110.x Medline

21. J. C. De la Concepcion, M. Franceschetti, A. Maqbool, H. Saitoh, R. Terauchi, S. Kamoun, M. J. Banfield, Polymorphic residues in rice NLRs expand binding and response to effectors of the blast pathogen. *Nat. Plants* **4**, 576–585 (2018). doi:10.1038/s41477-018-0194-x Medline

22. J. C. De la Concepcion, J. H. R. Maidment, A. Longya, G. Xiao, M. Franceschetti, M. J. Banfield, The allelic rice immune receptor Pikh confers extended resistance to strains of the blast fungus through a single polymorphism in the effector binding interface. *PLOS Pathog.* **17**, e1009368 (2021). doi:10.1371/journal.ppat.1009368 Medline

23. A. Białas, T. Langner, A. Harant, M. P. Contreras, C. E. Stevenson, D. M. Lawson, J. Sklenar, R. Kellner, M. J. Moscou, R. Terauchi, M. J. Banfield, S. Kamoun, Two NLR immune receptors acquired high-affinity binding to a fungal effector through

convergent evolution of their integrated domain. *eLife* **10**, e66961 (2021). doi:10.7554/eLife.66961 Medline

24. A. Białas, E. K. Zess, J. C. De la Concepcion, M. Franceschetti, H. G. Pennington, K. Yoshida, J. L. Upson, E. Chanclud, C.-H. Wu, T. Langner, A. Maqbool, F. A. Varden, L. Derevnina, K. Belhaj, K. Fujisaki, H. Saitoh, R. Terauchi, M. J. Banfield, S. Kamoun, Lessons in effector and NLR biology of plant-microbe systems. *Mol. Plant Microbe Interact.* **31**, 34–45 (2018). doi:10.1094/MPMI-08-17-0196-FI Medline

25. J. H. R. Maidment, M. Shimizu, S. Vera, M. Franceschetti, A. Longya, C. E. M. Stevenson, J. C. De la Concepcion, A. Białas, S. Kamoun, R. Terauchi, M. J. Banfield, Effector target-guided engineering of an integrated domain expands the disease resistance profile of a rice NLR immune receptor. bioRxiv 2022.06.14.496076 [Preprint] (2022). https://doi.org/10.1101/2022.06.14.496076.

26. A. R. Bentham, J. C. De la Concepcion, J. V. Benjumea, S. Jones, M. Mendel, J. Stubbs, C. E. M. Stevenson, J. H. R. Maidment, M. Youles, J. Kourelis, R. Zdrzałek, S. Kamoun, M. J. Banfield, Allelic compatibility in plant immune receptors facilitates engineering of new effector recognition specificities. bioRxiv 2022.10.10.511592 [Preprint] (2022). https://doi.org/10.1101/2022.10.10.511592.

27. K. Yoshida, H. Saitoh, S. Fujisawa, H. Kanzaki, H. Matsumura, K. Yoshida, Y. Tosa, I. Chuma, Y. Takano, J. Win, S. Kamoun, R. Terauchi, Association genetics reveals three novel avirulence genes from the rice blast fungal pathogen *Magnaporthe oryzae*. *Plant Cell* **21**, 1573–1591 (2009). doi:10.1105/tpc.109.066324 Medline

28. C. Hamers-Casterman, T. Atarhouch, S. Muyldermans, G. Robinson, C. Hamers, E. B. Songa, N. Bendahman, R. Hamers, Naturally occurring antibodies devoid of light chains. *Nature* **363**, 446–448 (1993). doi:10.1038/363446a0 Medline

29. A. S. Greenberg, D. Avila, M. Hughes, A. Hughes, E. C. McKinney, M. F. Flajnik, A new antigen receptor gene family that undergoes rearrangement and extensive somatic diversification in sharks. *Nature* **374**, 168–173 (1995). doi:10.1038/374168a0 Medline

30. S. Muyldermans, Nanobodies: Natural single-domain antibodies. *Annu. Rev. Biochem.* **82**, 775–797 (2013). doi:10.1146/annurev-biochem-063011-092449 Medline

31. D. Könning, S. Zielonka, J. Grzeschik, M. Empting, B. Valldorf, S. Krah, C. Schröter, C. Sellmann, B. Hock, H. Kolmar, Camelid and shark single domain antibodies: Structural features and therapeutic potential. *Curr. Opin. Struct. Biol.* **45**, 10–16 (2017). doi:10.1016/j.sbi.2016.10.019 Medline

32. J. G. Dingus, J. C. Y. Tang, R. Amamoto, G. K. Wallick, C. L. Cepko, A general approach for stabilizing nanobodies for intracellular expression. *eLife* **11**, e68253 (2022). doi:10.7554/eLife.68253 Medline

33. A. Kirchhofer, J. Helma, K. Schmidthals, C. Frauer, S. Cui, A. Karcher, M. Pellis, S. Muyldermans, C. S. Casas-Delucchi, M. C. Cardoso, H. Leonhardt, K.-P. Hopfner, U. Rothbauer, Modulation of protein properties in living cells using nanobodies. *Nat. Struct. Mol. Biol.* **17**, 133–138 (2010). doi:10.1038/nsmb.1727 Medline

34. P. C. Fridy, Y. Li, S. Keegan, M. K. Thompson, I. Nudelman, J. F. Scheid, M. Oeffinger, M. C. Nussenzweig, D. Fenyö, B. T. Chait, M. P. Rout, A robust pipeline for rapid production of versatile nanobody repertoires. *Nat. Methods* **11**, 1253–1260 (2014). doi:10.1038/nmeth.3170 Medline

35. J. C. De la Concepcion, J. Vega Benjumea, A. Białas, R. Terauchi, S. Kamoun, M. J. Banfield, Functional diversification gave rise to allelic specialization in a rice NLR immune receptor pair. *eLife* **10**, e71662 (2021). doi:10.7554/eLife.71662 Medline

36. R. Zdrzałek, S. Kamoun, R. Terauchi, H. Saitoh, M. J. Banfield, The rice NLR pair Pikp-1/Pikp-2 initiates cell death through receptor cooperation rather than negative regulation. *PLOS ONE* **15**, e0238616 (2020). doi:10.1371/journal.pone.0238616 Medline

37. J. Wang, J. Wang, M. Hu, S. Wu, J. Qi, G. Wang, Z. Han, Y. Qi, N. Gao, H.-W. Wang, J.-M. Zhou, J. Chai, Ligand-triggered allosteric ADP release primes a plant NLR complex. *Science* **364**, eaav5868 (2019). doi:10.1126/science.aav5868 Medline

38. S. P. Dinesh-Kumar, W.-H. Tham, B. J. Baker, Structure-function analysis of the tobacco mosaic virus resistance gene *N*. *Proc. Natl. Acad. Sci. U.S.A.* **97**, 14789–14794 (2000). doi:10.1073/pnas.97.26.14789 Medline

39. F. L. W. Takken, W. I. L. Tameling, To nibble at plant resistance proteins. *Science* **324**, 744–746 (2009). doi:10.1126/science.1171666 Medline

40. S. Marillonnet, C. Engler, V. Klimyuk, Y. Gleba, Potexvirus-derived replicon, Patent WO/2008/028661 (2008); https://patentscope.wipo.int/search/en/detail.jsf?docId=WO2008028661.

41. A. Bendahmane, K. Kanyuka, D. C. Baulcombe, The *Rx* gene from potato controls separate virus resistance and cell death responses. *Plant Cell* **11**, 781–792 (1999). doi:10.1105/tpc.11.5.781 Medline

42. R. Lu, I. Malcuit, P. Moffett, M. T. Ruiz, J. Peart, A.-J. Wu, J. P. Rathjen, A. Bendahmane, L. Day, D. C. Baulcombe, High throughput virus-induced gene silencing implicates heat shock protein 90 in plant disease resistance. *EMBO J.* **22**, 5690–5699 (2003). doi:10.1093/emboj/cdg546 Medline

43. S. S. Cruz, S. Chapman, A. G. Roberts, I. M. Roberts, D. A. Prior, K. J. Oparka, Assembly and movement of a plant virus carrying a green fluorescent protein overcoat. *Proc. Natl. Acad. Sci. U.S.A.* **93**, 6286–6290 (1996). doi:10.1073/pnas.93.13.6286 Medline

44. M. G. Goulden, B. A. Köhm, S. Santa Cruz, T. A. Kavanagh, D. C. Baulcombe, A feature of the coat protein of potato virus X affects both induced virus resistance in potato and viral fitness. *Virology* **197**, 293–302 (1993). doi:10.1006/viro.1993.1590 Medline

45. M. Luo, L. Xie, S. Chakraborty, A. Wang, O. Matny, M. Jugovich, J. A. Kolmer, T. Richardson, D. Bhatt, M. Hoque, M. Patpour, C. Sørensen, D. Ortiz, P. Dodds, B. Steuernagel, B. B. H. Wulff, N. M. Upadhyaya, R. Mago, S. Periyannan, E. Lagudah, R. Freedman, T. Lynne Reuber, B. J. Steffenson, M. Ayliffe, A five-transgene cassette confers broad-spectrum resistance to a fungal rust pathogen in wheat. *Nat. Biotechnol.* **39**, 561–566 (2021). doi:10.1038/s41587-020-00770-x Medline

46. S. Zhu, Y. Li, J. H. Vossen, R. G. F. Visser, E. Jacobsen, Functional stacking of three resistance genes against *Phytophthora infestans* in potato. *Transgenic Res.* **21**, 89–99 (2012). doi:10.1007/s11248-011-9510-1 Medline

47. M. Ghislain, A. A. Byarugaba, E. Magembe, A. Njoroge, C. Rivera, M. L. Román, J. C. Tovar, S. Gamboa, G. A. Forbes, J. F. Kreuze, A. Barekye, A. Kiggundu, Stacking three late blight resistance genes from wild species directly into African highland

potato varieties confers complete field resistance to local blight races. *Plant Biotechnol. J.* **17**, 1119–1129 (2019). doi:10.1111/pbi.13042 Medline

48. E. Chae, K. Bomblies, S.-T. Kim, D. Karelina, M. Zaidem, S. Ossowski, C. Martín-Pizarro, R. A. E. Laitinen, B. A. Rowan, H. Tenenboim, S. Lechner, M. Demar, A. Habring-Müller, C. Lanz, G. Rätsch, D. Weigel, Species-wide genetic incompatibility analysis identifies immune genes as hot spots of deleterious epistasis. *Cell* **159**, 1341–1351 (2014). doi:10.1016/j.cell.2014.10.049 Medline

49. D. T. N. Tran, E.-H. Chung, A. Habring-Müller, M. Demar, R. Schwab, J. L. Dangl, D. Weigel, E. Chae, Activation of a plant NLR complex through heteromeric association with an autoimmune risk variant of another NLR. *Curr. Biol.* **27**, 1148–1160 (2017). doi:10.1016/j.cub.2017.03.018 Medline

50. S. Hurni, S. Brunner, D. Stirnweis, G. Herren, D. Peditto, R. A. McIntosh, B. Keller, The powdery mildew resistance gene *Pm8* derived from rye is suppressed by its wheat ortholog *Pm3*. *Plant J.* **79**, 904–913 (2014). doi:10.1111/tpj.12593 Medline

51. Z. Zhang, Y. Wang, Y. Ding, M. Hattori, Structure-based engineering of anti-GFP nanobody tandems as ultra-high-affinity reagents for purification. *Sci. Rep.* **10**, 6239 (2020). doi:10.1038/s41598-020-62606-7 Medline

52. Z. Wang, L. Li, R. Hu, P. Zhong, Y. Zhang, S. Cheng, H. Jiang, R. Liu, Y. Ding, Structural insights into the binding of nanobodies LaM2 and LaM4 to the red fluorescent protein mCherry. *Protein Sci.* **30**, 2298–2309 (2021). doi:10.1002/pro.4194 Medline

53. D. MacLean, besthr - Generating Bootstrap Estimation Distributions of HR Data, Github (2020); https://github.com/TeamMacLean/besthr.

54. E. Weber, C. Engler, R. Gruetzner, S. Werner, S. Marillonnet, A modular cloning system for standardized assembly of multigene constructs. *PLOS ONE* **6**, e16765 (2011). doi:10.1371/journal.pone.0016765 Medline

55. C. Engler, M. Youles, R. Gruetzner, T.-M. Ehnert, S. Werner, J. D. G. Jones, N. J. Patron, S. Marillonnet, A golden gate modular cloning toolbox for plants. *ACS Synth. Biol.* **3**, 839–843 (2014). doi:10.1021/sb4001504 Medline

56. D. Saerens, M. Pellis, R. Loris, E. Pardon, M. Dumoulin, A. Matagne, L. Wyns, S. Muyldermans, K. Conrath, Identification of a universal VHH framework to graft non-canonical antigen-binding loops of camel single-domain antibodies. *J. Mol. Biol.* **352**, 597–607 (2005). doi:10.1016/j.jmb.2005.07.038 Medline

57. U. Rothbauer, K. Zolghadr, S. Tillib, D. Nowak, L. Schermelleh, A. Gahl, N. Backmann, K. Conrath, S. Muyldermans, M. C. Cardoso, H. Leonhardt, Targeting and tracing antigens in live cells with fluorescent nanobodies. *Nat. Methods* **3**, 887–889 (2006). doi:10.1038/nmeth953 Medline

58. R. A. L. Van der Hoorn, F. Laurent, R. Roth, P. J. G. M. De Wit, Agroinfiltration is a versatile tool that facilitates comparative analyses of *Avr9/Cf-9*-induced and *Avr4/Cf-4*-induced necrosis. *Mol. Plant Microbe Interact.* **13**, 439–446 (2000). doi:10.1094/MPMI.2000.13.4.439 Medline

59. R. A. L. van der Hoorn, B. B. H. Wulff, S. Rivas, M. C. Durrant, A. van der Ploeg, P. J. G. M. de Wit, J. D. G. Jones, Structure-function analysis of Cf-9, a receptor-like protein with extracytoplasmic leucine-rich repeats. *Plant Cell* **17**, 1000–1015 (2005). doi:10.1105/tpc.104.028118 Medline

60. H. Adachi, M. P. Contreras, A. Harant, C.-H. Wu, L. Derevnina, T. Sakai, C. Duggan, E. Moratto, T. O. Bozkurt, A. Maqbool, J. Win, S. Kamoun, An N-terminal motif in NLR immune receptors is functionally conserved across distantly related plant species. *eLife* **8**, e49956 (2019). doi:10.7554/eLife.49956 Medline

61. C. Ginestet, ggplot2: Elegant graphics for data analysis. *J. R. Stat. Soc. Ser. A Stat. Soc.* **174**, 245–246 (2011). doi:10.1111/j.1467-985X.2010.00676_9.x

62. T. Clemente, in *Agrobacterium Protocols: Volume I*, K. Wang, Ed., vol. 343 of *Methods in Molecular Biology*, J. M. Walker, Ed. (Humana Press, 2006), pp. 143–154.

63. A. Signorell, DescTools - Tools for descriptive statistics and exploratory data analysis, Github (2021); https://github.com/AndriSignorell/DescTools.

64. J. Du, H. Rietman, V. G. A. A. Vleeshouwers, Agroinfiltration and PVX agroinfection in potato and *Nicotiana benthamiana*. *J. Vis. Exp.* **83**, e50971 (2014). doi:10.3791/50971 Medline